Polyimide Encapsulated Lithium-Rich Cathode Material for High Voltage Lithium-Ion Battery

Jie Zhang, Qingwen Lu, Jianhua Fang, Jiulin Wang,* Jun Yang, and Yanna NuLi

School of Chemistry and Chemical Engineering, Shanghai Jiao Tong University, 800 Dongchuan Road, Shanghai 200240, China

Ⓢ Supporting Information

ABSTRACT: Lithium-rich materials represented by xLi$_2$MnO$_3$·$(1 − x)$LiMO$_2$ (M = Mn, Co, Ni) are attractive cathode materials for lithium-ion battery due to their high specific energy and low cost. However, some drawbacks of these materials such as poor cycle and rate capability remain to be addressed before applications. In this study, a thin polyimide (PI) layer is coated on the surface of Li$_{1.2}$Ni$_{0.13}$Mn$_{0.54}$Co$_{0.13}$O$_2$ (LNMCO) by a polyamic acid (PAA) precursor with subsequently thermal imidization process. X-ray diffraction (XRD), scanning electron microscopy (SEM), and high-resolution transmission electron microscopy (HR-TEM) results confirm the successful formation of a PI layer (∼3 nm) on the surface of LNMCO without destruction of its main structure. X-ray photoelectron spectroscopy (XPS) spectra show a slight shift of the Mn valence state from Mn(IV) to Mn(III) in the PI-LNMCO treated at 450 °C, elucidating that charge transfer takes place between the PI layer and LNMCO surface. Electrochemical performances of LNMCO including cyclic stability and rate capability are evidently improved by coating a PI nanolayer, which effectively separates the cathode material from the electrolyte and stabilizes their interface at high voltage.

KEYWORDS: lithium-rich material, surface coating, polyimide, interfacial reaction, lithium-ion battery
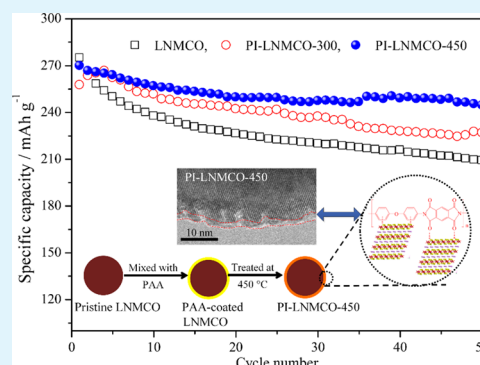
1. INTRODUCTION

Presently, lithium-ion batteries (LIBs) have been used in portable electronic devices and are taking a leading role to power hybrid electric vehicles (HEVs) and electric vehicles (EVs) which demand both high energy and power densities.[1] Traditional hexagonal layered oxide (e.g., LiMO$_2$, M = Co, Mn, Ni[2−4]), cubic spinel (e.g., LiMn$_2$O$_4$[5,6]), and olivine structures (e.g., LiFePO$_4$[7]) are the most widely used cathode materials. However, discharge capacities of the aforementioned cathode materials, which limit the maximum to 200 mAh g$^{−1}$, cannot fully meet the demands of HEVs and EVs. Thus, the development for low cost and high energy density cathode materials is of great importance for the next generation of LIBs. Lithium-rich materials represented by xLi$_2$MnO$_3$·$(1 − x)$LiMO$_2$ (M = Mn, Co, Ni) have been currently investigated as promising candidates for lithium-ion batteries due to their high capacity (ca. 250 mAh g$^{−1}$) and low cost.[8,9] However, some significant drawbacks of these materials, such as high first cycle irreversibility, poor cyclic stability, poor rate capability, and severe voltage plateau, decrease with cycling and require being well addressed before their practical applications.[10−15]

One effective method to resolve the aforementioned problems of lithium-rich materials is surface modification with coating materials such as Al$_2$O$_3$,[16] ZrO$_2$,[17] MoO$_3$,[18] and AlF$_3$,[19] which reduces the irreversible capacity in the initial cycle and improves cyclic stability by suppressing elimination of oxygen ion vacancies and parasitic reactions at high voltage (≥4.5 V).

However, these inorganic materials often present as inert and discontinuous layers onto the surface of lithium-rich materials.

Recently, polyimide (PI) encapsulation generated from polyamic acid (PAA) was reported to improve the rate performance and cyclic stability of LiCoO$_2$[20,21] and LiNi$_{1/3}$Mn$_{1/3}$Co$_{1/3}$O$_2$.[22] The high polarity and outstanding film-forming capability of PAA, plus its strong affinity to transitional metal oxide surfaces, may contribute to a facile formation of a nanometer-thick, highly continuous, and ionic-conductive PI encapsulating layer on the surface of active materials.[23] In this paper, we first prepared Li$_{1.2}$Ni$_{0.13}$Mn$_{0.54}$Co$_{0.13}$O$_2$ (LNMCO) with PI nanocoating which remarkably enhanced the electrochemical performances of LNMCO including cyclic stability and rate capability.

2. EXPERIMENTAL SECTION

2.1. Synthesis of Li$_{1.2}$Ni$_{0.13}$Mn$_{0.54}$Co$_{0.13}$O$_2$. The Li$_{1.2}$Ni$_{0.13}$Mn$_{0.54}$Co$_{0.13}$O$_2$ material was synthesized by a spray drying-pyrolysis method.[24] In detail, the stoichiometric amounts of Ni(CH$_3$COO)$_2$·4H$_2$O, Co(CH$_3$COO)$_2$·4H$_2$O, Mn(CH$_3$COO)$_2$·4H$_2$O, and LiCH$_3$COO·2H$_2$O as starting materials and citric acid as chelating agent were dissolved in distilled water. The mole ratio of citric acid to metal ion was 2:1. The pH value of the mixed solution was adjusted by ammonia solution to 7. The final solution was pumped into a spray drying instrument (B-290, Buchi). The dried

precursor was precalcined at 400 °C for 6 h, then grounded and fired at 900 °C for 12 h in air to obtain the pristine $Li_{1.2}Ni_{0.13}Mn_{0.54}Co_{0.13}O_2$.

2.2. Synthesis of Polyamic Acid (PAA). Synthesis of the PAA has been described in a previous study.[25] The two-component PAA solution was prepared using pyromellitic dianhydride (PMDA) and 4,4′-diaminodiphenyl ether (ODA) as reactants and dimethylacetamide (DMAC) as a solvent under an argon atmosphere. The mole ratio of PMDA/ODA was fixed at 1. In detail, ODA (0.957 g, 4.78 mmol) was completely dissolved in 18 g of DMAC with stirring in a three-neck flask at room temperature. PMDA (1.043 g, 4.78 mmol) was added into ODA solution in three aliquots in 30 min. Then, the above mixture was stirred for another 8 h to form the 10.0 wt % PAA solution.

2.3. Preparation of PI-Coated $Li_{1.2}Ni_{0.13}Mn_{0.54}Co_{0.13}O_2$. The pristine $Li_{1.2}Ni_{0.13}Mn_{0.54}Co_{0.13}O_2$ powder was added to the 1.0 wt % PAA solution which was diluted by DMAC then subjected to vigorous stirring for 1 h under an argon atmosphere. Subsequently, the powder was centrifuged and vacuum-dried at room temperature overnight. Meanwhile, the PAA solution (10.0 wt %) was evenly coated on the surface of glass to form a PAA membrane for comparison. In order to convert the PAA to PI, the PAA membrane and PAA-coated $Li_{1.2}Ni_{0.13}Mn_{0.54}Co_{0.13}O_2$ powder were thermally cured via two kinds of stepwise imidization processes under an argon atmosphere, that is, treated at 80 °C for 120 min and at 150 °C for 60 min and followed by a step by step thermal treatment for 60 min with a step increment of 50 °C until it reaches 300 or 450 °C, respectively. Hereinafter, $Li_{1.2}Ni_{0.13}Mn_{0.54}Co_{0.13}O_2$, the PI membrane, and PI-coated $Li_{1.2}Ni_{0.13}Mn_{0.54}Co_{0.13}O_2$ treated at 300 or 450 °C are abbreviated as LNMCO, PI-X, and PI-LNMCO-X (X = 300 or 450), respectively.

2.4. Sample Analysis. The crystal structure of the prepared samples was analyzed with powder X-ray diffraction (XRD) using a D8 advance X-ray diffractometer (Bruker) with Cu Kα radiation operated at 40 kV and 40 mA. The data were collected on the 2θ range from 10° to 90° at a scan speed of 6 ° min⁻¹. The surface morphology was observed by a field emission scanning electron microscope (FE-SEM, S-4800, Hitachi) and a high-resolution transmission electron microscope (HR-TEM, JEM-2100, JEOL). Fourier transform infrared spectroscopy (FT-IR) was measured on a Spectrum 100 (PerkinElmer) using the KBr disk. LNMCO and PI-LNMCO were characterized via a Raman monochromator (InVia-Reflex, Renishaw). The chemical valences of C, N, O, Mn, Co, and Ni in PI-X membranes, LNMCO, and PI-LNMCO-X powders (X represents heating treatment temperature, 300 or 450 °C) were analyzed by X-ray photoelectron spectroscopy (XPS, ESCALAB 250, Thermo) with the Al Ka line as an X-ray source.

2.5. Electrochemical Measurements. The working cathode was fabricated by coating a 1-methyl-2-pyrrolidinone (NMP) based slurry consisting of 80 wt % active material, 10 wt % Super P, and 10 wt % polyvinylidene difluoride (PVDF) on aluminum foil. Electrochemical measurement was tested in coin-type cell (CR2016) consisting of a cathode, a PE separator, and a lithium metal anode with 1 M $LiPF_6$ in ethylene carbonate/dimethyl carbonate (1:1 by volume) as electrolyte. All cells were assembled in an argon-filled glovebox. The galvanostatic charge/discharge and rate tests were conducted on a Land CT2001 battery test system in a voltage range of 2.0−4.8 V at 30 °C. Electrochemical impedance spectroscopy (EIS) was conducted on a CHI650C in the frequency range of 0.01 Hz to 100 kHz with the amplitude of 5 mV.

3. RESULTS AND DISSCUSSION

3.1. Structure, Morphology, and Interfacial Reactions. The structure of pristine LNMCO is a perfect integration of layered $LiNi_{1/3}Mn_{1/3}Co_{1/3}O_2$ (Figure 1a) and layered Li_2MnO_3 (Figure 1b) structures at the atomic level, due to their similar cubic closed-packed (ccp) layers having an interlayer spacing of ~4.7 Å, (001) for layered Li_2MnO_3 and (003) for layered $LiNi_{1/3}Mn_{1/3}Co_{1/3}O_2$.[26] Figure 1c shows the XRD patterns of the LNMCO and PI-LNMCO powders. The main peaks of the

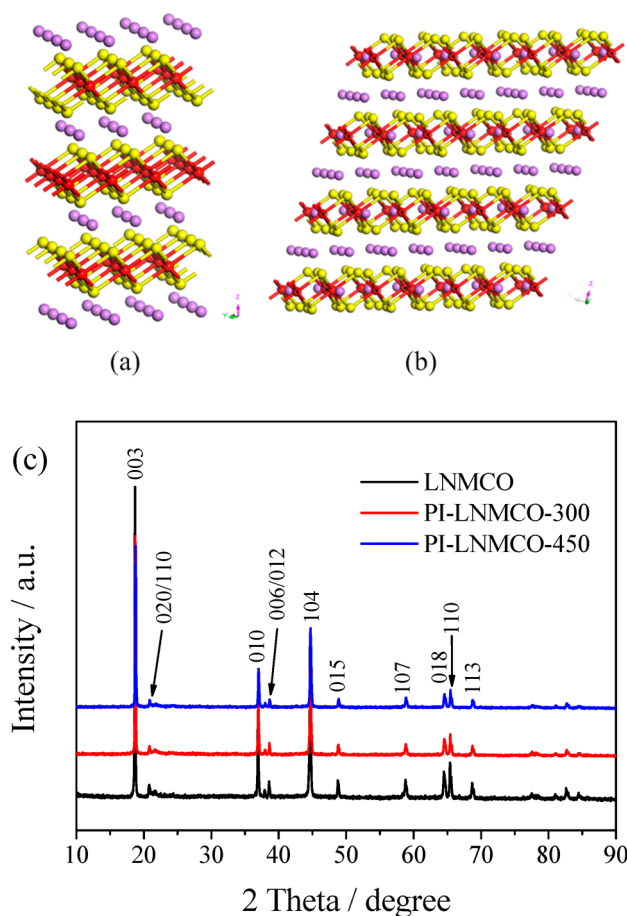**Figure 1.** Crystal structures of the hexagonal unit cell of $LiNi_{1/3}Mn_{1/3}Co_{1/3}O_2$ (a) and monoclinic unit cell of Li_2MnO_3 (b). XRD patterns of the pristine LNMCO and PI-LNMCO powders (c).

pristine sample can be indexed to a layered structure of hexagonal α-NaFeO$_2$ type with space group $R\bar{3}m$. The weak peaks between 20° and 25° are consistent with the LiMn$_6$ cation arrangement that occurs in the transition metal layer of Li_2MnO_3. Furthermore, distinct splitting (006)/(102) and (108)/(110) peaks observed in all the XRD patterns indicate the formation of a typical layered structure.[27,28] The XRD patterns of PI-LNMCO samples are actually identical to that of pristine LNMCO, which indicate that the main structure of LNMCO remained unchanged after PI coating. No peak of PI was observed due to its low content.

The SEM images of the LNMCO and PI-LNMCO materials are shown in Figure 2. Figure 2a and 2b reveal that the polyhedral nanoparticle of pristine LNMCO powder is relatively uniform in the range from 200 to 400 nm. The sharp edges and smooth planes indicate that the LNMCO material is highly crystallized, which is consistent with the XRD results. Comparing with the bare LNMCO, PI-LNMCO-300 (Figure 2c) and PI-LNMCO-450 (Figure 2d) are characterized with a rougher surface due to the coverage of the PI layer on the surface of the LNMCO particle. TEM results demonstrate that the morphology of the LMCNO particle clearly changed after PI coating, as shown in Figure 3. Apparent lattice fringes with a space width of 4.7 Å can be observed in pristine LNMCO, corresponding to the interplanar spacing of the (003) planes. By contrast, a ~3 nm thin and compact PI layer is covered on the surface of LNMCO particles which keep its
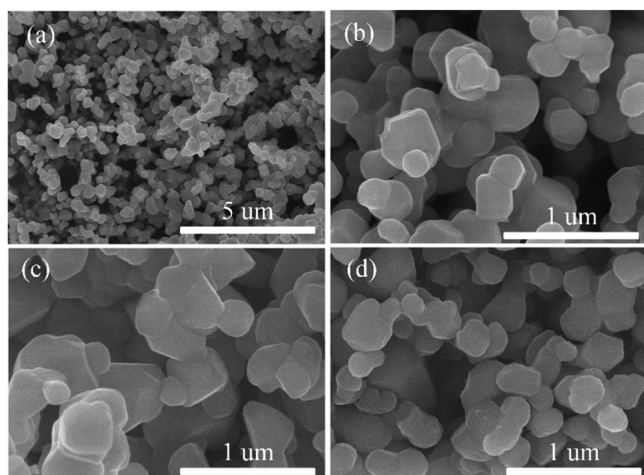
Figure 2. SEM images of pristine LNMCO (a and b), PI-LNMCO-300 (c), and PI-LNMCO-450 (d) samples.
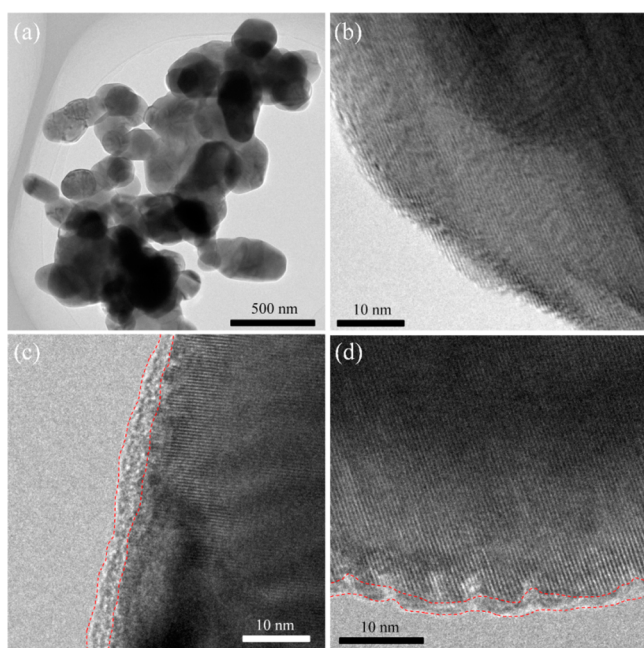

Figure 3. TEM images of pristine LNMCO (a and b), PI-LNMCO-300 (c), and PI-LNMCO-450 (d) samples.
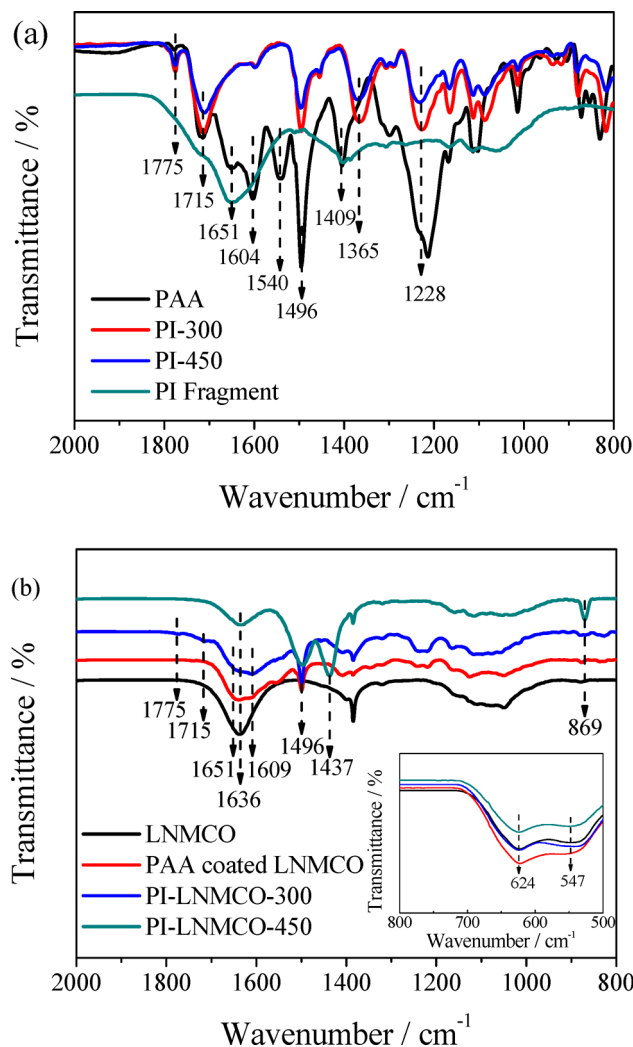

Figure 4. FT-IR spectra of PAA membranes, PI membranes, and PI fragments obtained by dissolving the LNMCO component from PI-LNMC-450 (a) and pristine LNMCO, PAA-coated LNMCO, and PI-LNMCO powders (b).

well-defined fringe patterns in the inner of the PI-LNMCO particles (Figure 3c and 3d). SEM and TEM images indicate that the PI coating layer was uniformly covered on the surface of PI-LNMCO without damage to its inner structure of LNMCO.

To clarify the formation process of the PI layer on the surface of LNMCO, FT-IR spectra were measured to analyze the chemical bonds in pure PAA, PI membranes, LNMCO, PAA-coated LNMCO, PI-LNMCO powders, and PI fragments obtained by dissolving PI-LNMCO-450 with HCl solution at 50 °C. In the FT-IR spectrum of the PAA membrane (Figure 4a), the peak at 1715 cm^{-1} is corresponding to the C=O vibrations of carboxylic acid groups; the peak at 1651 cm^{-1} is assigned to the vibrational mode of the amide groups; and the peak at 1496 cm^{-1} is attributed to the benzene ring, respectively.[25,29] After a thermal imidization process, the characteristic peaks of PI including the C=O bond at 1775

cm^{-1} (asymmetric stretch) and 1711 cm^{-1} (symmetric stretch) and the C−N bond at 1365 cm^{-1} are clearly observable in Figure 4a,[25,30] and the FT-IR spectra present no significant difference between PI-300 and PI-450. After a thermal imidization process at 300 °C, the PAA membrane was almost completely converted into the PI membrane which is stable at 450 °C, as indicated in Figure 4a.

LNMCO exhibited two separated peaks at 624 and 547 cm^{-1} representing the M−O (M = Mn, Co, Ni) asymmetrical stretching of LNMCO,[31] which kept unchanged after surface coating, as shown in Figure 4b (inset). For the PAA-coated LNMCO, an apparent peak appears at 1496 cm^{-1} ascribed to the benzene ring of PAA, and a weak peak appears at 1651 cm^{-1} assigned to the vibrational mode of amide groups of PAA, which confirm the successful PAA coating on LNMCO. After thermal imidization at 300 °C, weak peaks at 1775 and 1715 cm^{-1} assigned to imine groups of PI appeared, indicating the formation of PI on the surface of PI-LNMCO-300. However, the C=O bond at 1651 cm^{-1} ascribed to PAA still is detectable, which elucidates that only partial PAA was converted to PI through the thermal treatment at 300 °C.
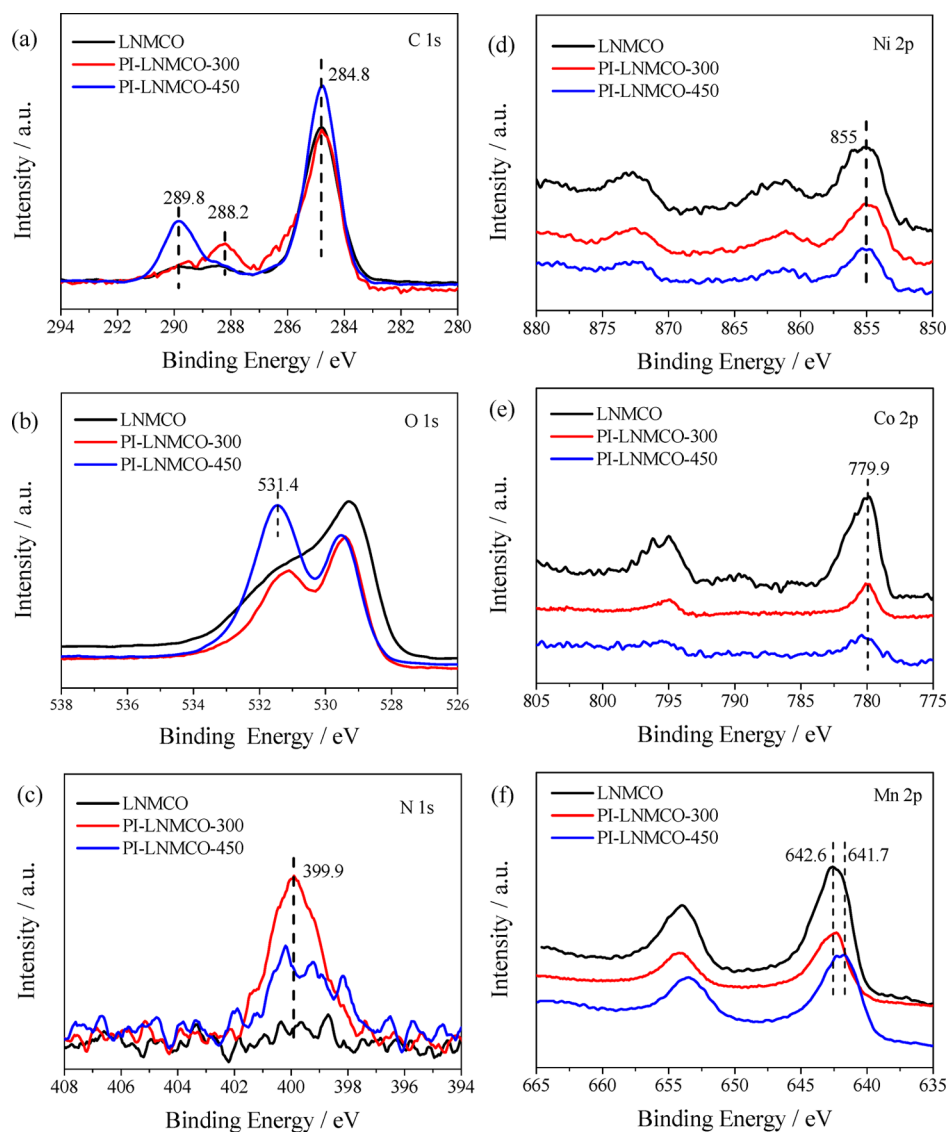
Figure 5. XPS spectra of C 1s (a), O 1s (b), N 1s (c), Ni 2p (d), Co 2p (e), and Mn 2p (f) of the pristine LNMCO, PI-LNMCO-300, and PI-LNMCO-450 materials.

Compared with the FT-IR spectrum of PI-300 (Figure 4a), it can be inferred that the thermal imidization process of the PAA coating layer was greatly affected by LNMCO. Of note, when the thermal imidization temperature reaches 450 °C, it is hard to detect characteristic peaks of PI, while three remarkable peaks appear at 1496, 1437, and 869 cm^{-1}. Due to the small amount of PI that exists on the surface of PI-LNMCO-450, the three significant peaks might be the response of some interactions between the PI layer and LNMCO during the thermal imidization process approaching 450 °C,[32] which will be discussed later.

Furthermore, in order to exclude the signals from LNMCO and confirm the existence of the PI layer on the surface of PI-LNMCO-450, the LNMCO component of PI-LNMCO-450 was dissolved by 2 M HCl at 50 °C. The residual was washed by distilled water several times and detected by FT-IR. As shown in Figure 4a, a broad peak appears in a wide range from 1830 to 1520 cm^{-1} due to the overlap of the C=O bond from PI (1775 and 1715 cm^{-1}) and the C=O bond from PAA (1715 and 1651 cm^{-1}). Considering the possibility of PI hydrolysis during the dissolution of LNMCO by HCl at 50 °C,

the coating layer on the PI-LNMCO-450 was speculated to be a PI layer.

XPS was adopted to analyze the surface interaction between the PI layer and LNMCO in PI-LNMCO samples. The XPS spectra of C 1s, O 1s, N 1s, Ni 2p, Co 2p, and Mn 2p in the PI membranes and LNMCO and PI-LNMCO samples are shown in the Supporting Information Figure S1 and Figure 5. The XPS spectra of PI-300 and PI-450 membranes in Figure S1 consist of a typical C=O bond (288.7 eV in C 1s and 532.0 eV in O 1s) and C−N bond (285.6 eV in C 1s and 400.6 eV in N 1s) of PI.[33] Similar C=O bond and C−N bond of PI are also observed in the PI-LNMCO in Figure 5. The XPS spectra of pristine LNMCO shows the binding energy of peaks in Mn 2p (642.6 eV), Ni 2p (855.0 eV), and Co 2p (779.9 eV), which indicates that the valence state of Mn is between +3 and +4, and Ni and Co are +2 and +3, respectively.[31,34,35] After the PI layer coating, the intensities of the Mn 2p, Ni 2p, and Co 2p spectra are significantly reduced due to PI encapsulation. The valence states of Co and Ni in PI-LNMCO-450 are consistent with that of pristine LNMCO, while the Mn 2p spectrum shows an obvious shift to lower binding energy (from 642.6 to

641.7 eV) indicating the Mn atom absorbed the electron during the PI coating. Besides, the C=O bond at 288.7 eV in PI membranes shifts to a higher binding energy at 289.8 eV in the PI-LNMCO-450.

It is well-known that PI films show considerable color change from pale yellow to deep brown owing to intramolecular or intermolecular charge transfer interactions between electron-donor and electron-acceptor moieties.[36] Mn(IV) in Li_2MnO_3 has a strong electron-withdrawing capability, while the C=O bond and benzene ring in the PI layer have electron-donating ability. Therefore, we speculated that the shift of the Mn 2p spectrum to lower binding energy and the shift of the C=O bond in the C 1s spectrum to higher binding energy may be due to the charge transfer between LNMCO and the PI layer. Three new peaks (1496, 1437, and 869 cm^{-1}) in the PI-LNMCO-450 as described in the FT-IR spectra (Figure 4b) may also be attributed to the charge transfer of lone pair electrons on the C=O bond and delocalized electrons on the benzene ring in the PI layer to Mn(IV) in Li_2MnO_3 and formation of weak Mn(III)···O and Mn(III)···benzene ring interactions.[31,32,36]

No D-band for amorphous carbon (~1346 cm^{-1}) or G-band for graphitic form (~1596 cm^{-1}) could be detected in the Raman spectra in the range of 1200−1800 cm^{-1} shown in the Supporting Information Figure S2, indicating that no carbonization of PAA or PI happened on the surface of LNMCO at 450 °C.

On the basis of the above discussion, the PI coating process and possible interface structure of PI-LNMCO-450 material are schematically illustrated in Figure 6. The strong affinity
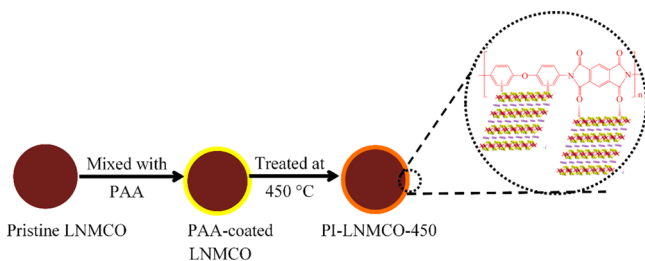

Figure 6. Schematic illustrations of the PI coating process and possible interfacial structure for PI-LNMCO-450.

between PAA and LNMCO contributes to a nanometer-thick and highly continuous PAA layer covered on LNMCO. Through a thermal imidization process, the nano PAA coating layer was ultimately converted to a PI layer. Differing from the PAA membrane, the PI coating layer on the surface of LNMCO undergoes a remarkable interfacial reaction in the conversion process to PI. Charge transfer between the electron donors (C=O bond and benzene ring in the PI layer) and electron acceptor (surface Mn(IV) in Li_2MnO_3) might happen at 450 °C to form weak Mn(III)···O and Mn(III)···benzene ring interactions.

3.2. Electrochemical Properties. Figure 7a shows the initial charge/discharge profiles of LNMCO, PI-LNMCO-300, and PI-LNMCO-450/Li cells at a current density of 20 mA g^{-1} between 2.0 and 4.8 V. The LNMCO shows a typical charge/discharge profile of lithium-rich material. During the first charge, lithium extraction from the lithium layer ascribed to the oxidation of Ni^{2+}/Ni^{4+} and Co^{3+}/Co^{4+} occurs between 3.9 and 4.4 V, followed by removal of superfluous lithium from the transition metal layer along with simultaneous oxygen evolution
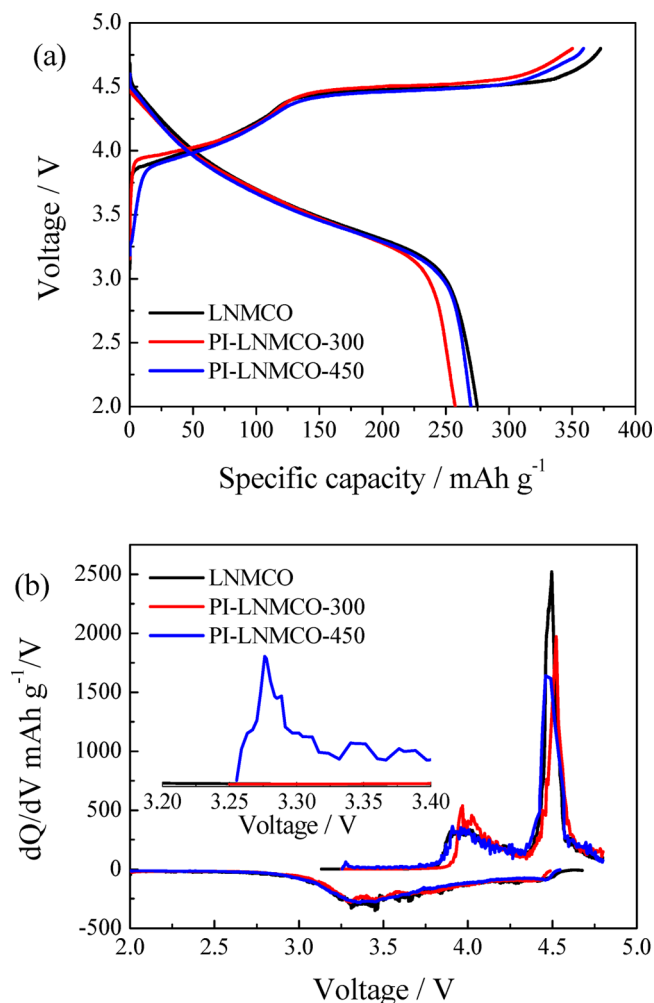

Figure 7. Initial charge/discharge curves (a) and corresponding dQ/dV profiles of LNMCO, PI-LNMCO-300, and PI-LNMCO-450 (b).

at the voltage of 4.5 V and oxidation of electrolyte at high voltage (≥4.5 V).[24] Compared with the pristine LNMCO, PI-LNMCO-300 and PI-LNMCO-450 exhibited slightly different charge/discharge curves. The PI-LNMCO-300 material delivers a discharge capacity of 257.5 mAh g^{-1} much lower than that of pristine material (274.9 mAh g^{-1}) due to the increment of the electrode/electrolyte interface resistance by PAA encapsulation on the surface, which impedes Li^+ diffusion from bulk to electrolyte to some extent. During the initial charge process of PI-LNMCO-450, a new slope ascribed to the oxidation of newly formed Mn(III) occurs in the voltage range of 3.2 and 3.8 V, and the PI-LNMCO-450 material delivers a discharge capacity of 269.8 mAh g^{-1}.

The dQ/dV profiles were performed to further understand the electrochemical process of LNMCO, PI-LNMCO-300, and PI-LNMCO-450 materials. Figure 7b shows the corresponding dQ/dV profiles of initial charge/discharge curves of LNMCO, PI-LNMCO-300, and PI-LNMCO-450. There are two anodic peaks in the initial oxidation section of LNMCO, one at ~4.0 V and another at about 4.50 V. The anodic peaks at ~4.0 V can be ascribed to the extraction of Li^+ ions from the $LiNi_{1/3}Co_{1/3}Mn_{1/3}O_2$ region accompanied by Ni oxidation from Ni^{2+} to Ni^{4+} and Co oxidation from Co^{3+} to Co^{4+}. The second sharp peak at 4.50 V corresponds to the irreversible loss of Li_2O from the Li_2MnO_3 phase to form a layered MnO_2
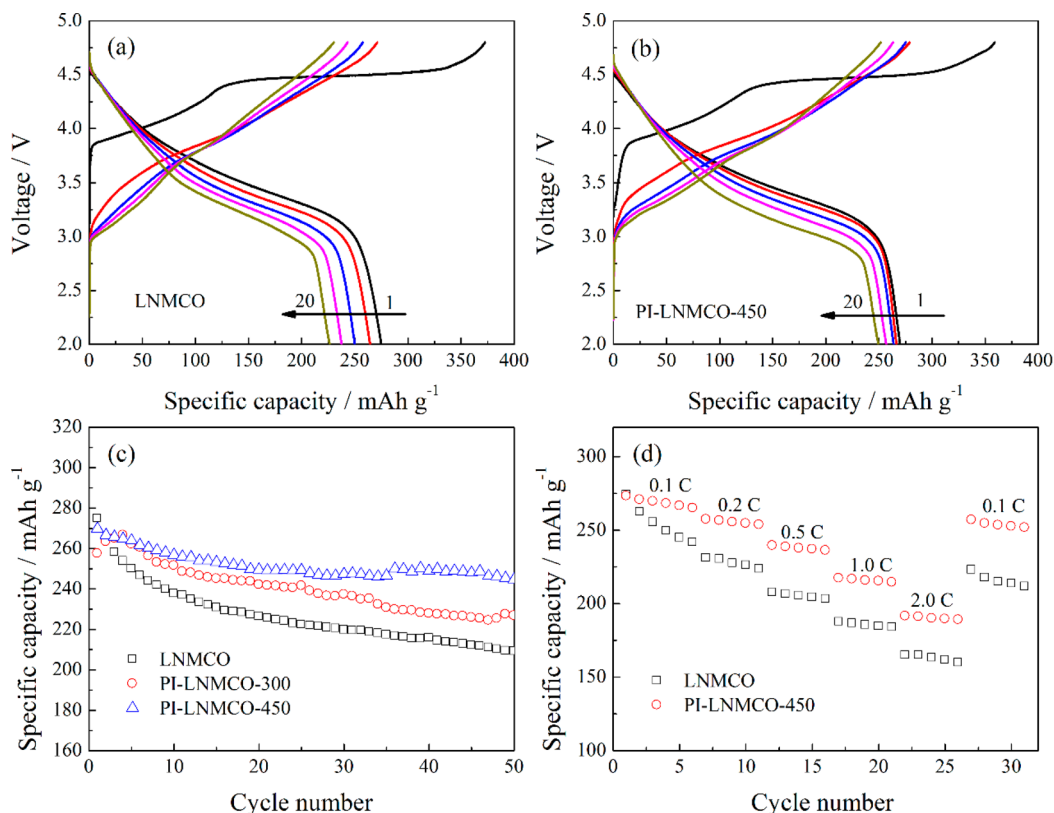
Figure 8. Comparison of the 1st, 2nd, 5th, 10th, and 20th charge/discharge curves of pristine LNMCO (a) and PI-LNMCO-450 (b); their cyclic behaviors (c) and rate performances (d) in the voltage range of 2.0−4.8 V.

component.[37−39] For the initial dQ/dV profile of the PI-LNMCO-450 sample, a new anodic peak corresponding to newly formed Mn(III) appeared at 3.29 V, which was consistent with the initial charge process. In the initial reduction section, the voltage range from 4.5 to 3.5 V corresponded to the reduction of Ni^{4+} and Co^{4+}, whereas the reduction peak at ∼3.30 V was assigned to the reduction of Mn(IV) to Mn(III).[40,41]

The LNMCO, PI-LNMCO-300, and PI-LNMCO-450/Li cells were cycled between 2.0 and 4.8 V at a specific current density of 20 mA g^{-1} to evaluate the effect of the PI layer on their cyclic behaviors. As shown in Figure 8a, the discharge capacity of LNMCO gradually decreased with cycling, which might derive from the surface deterioration of LNMCO nanomaterial due to side reactions at the interface between the electrode and electrolyte at high voltage.[24,42] By contrast, the PI-LNMCO-450 electrode (Figure 8b) exhibits fairly stable discharge capacity. Figure 8c shows that the PI-LNMCO-450 electrode delivered a higher discharge capacity of 244.6 mA h g^{-1} with a retention of 90.6% after 50 cycles. However, only 226.8 mAh g^{-1}, equal to 78% of its initial capacity, left for LNMCO. The rate capability of the pristine LNMCO and PI-LNMCO-450 samples was tested at various discharge rates from 0.1 to 2.0C with a constant charge rate (0.1C) in a voltage range of 2.0−4.8 V. One C rate is equal to a current density of 200 mA g^{-1} in our definition. The PI-LNMCO-450 electrode delivered a discharge capacity of 273.2, 257.4, 239.5, 217.3, and 191.5 mA h g^{-1} at 0.1, 0.2, 0.5, 1.0, and 2.0 C, respectively (Figure 8d), whereas the LNMCO electrode showed discharge capacity of 274.1, 231.1, 207.7, 187.7, and 164.9 mA h g^{-1} at the similar discharge rates. It is noteworthy that when the current was reduced back to 0.1 C the discharge capacity of the

PI-LNMCO-450 electrode recovered to 257.0 mAh g^{-1}, while the LNMCO electrode only returned to 223.0 mA h g^{-1}. Obviously, the PI-LNMCO-450 electrode exhibited a higher rate capability than that of the pristine LNMCO electrode.

The much improved cyclic stability and rate capabilities for the PI-LNMCO-450 electrode are possibly due to both a partial reduction of Mn from Mn(IV) to Mn(III) and the presence of a PI layer on its surface. Since the spinel structure with occupancy of octahedral sites by Mn at different valences (Mn(III) and Mn(IV)) has been suggested to benefit the migration of polarons,[43,44] the slight shift of Mn from Mn(IV) to Mn(III) after the PI coating process likely takes on the responsibility of a high rate performance. Meanwhile, the PI coating layer can effectively stabilize the electrode/electrolyte interface and alleviate decomposition of electrolyte at high voltage.[22,45]

To further explain the electrochemical improvements on LNMCO by coating a PI layer, electrochemical impedance spectroscopy (EIS) was performed at 3.0 V vs Li/Li$^+$ under a frequency of 0.01 Hz ∼ 100 kHz to identify the variations of impedance in discharged LNMCO and PI-LNMCO-450 electrodes. The Nyquist plots of these electrodes after the initial and 50th cycle are shown in Figure 9. As illustrated, a high-frequency semicircle and a large arc in the middle and low-frequency are observed in the LNMCO and PI-LNMCO-450 electrodes. The semicircle in the high-frequency region corresponds to the resistance of the SEI film, and the semicircle in the middle-frequency region is assigned to surface charge transfer resistance. These impedance spectra are analyzed by Zsimpwin software using the equivalent circuit (Figure 9c), where Re stands for internal resistance; R_f and CPE_f represent the resistance and double-layer capacitance of the SEI layer; R_{ct}
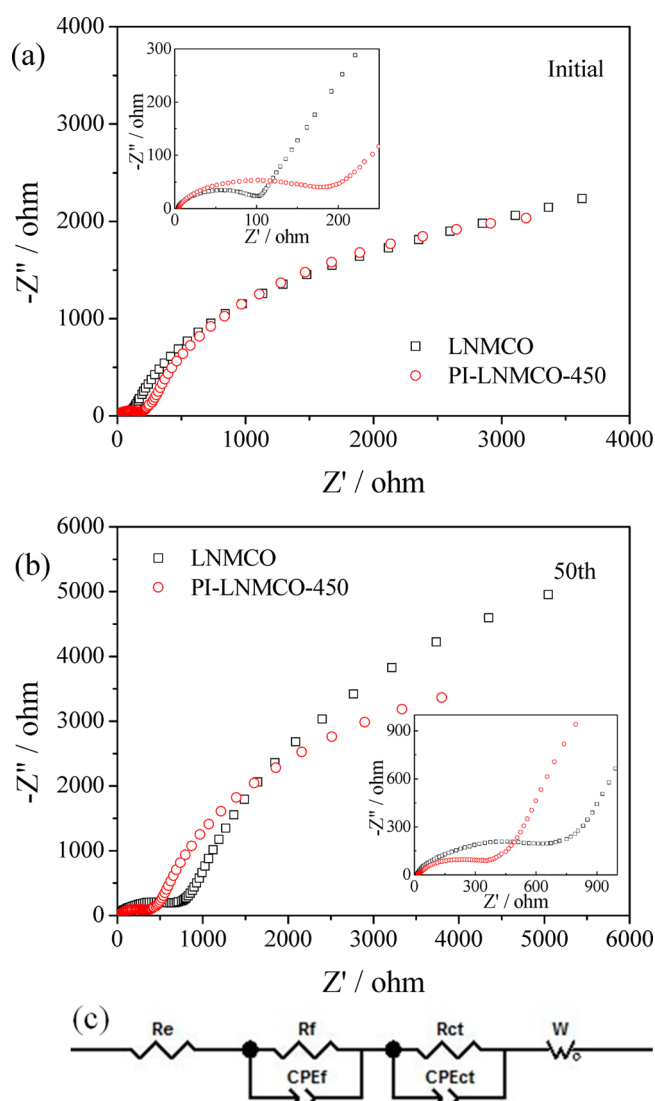
Figure 9. Nyquist plots of pristine LNMCO and PI-LNMCO-450 electrodes after the initial (a) and 50th cycle (b). The equivalent circuit used in this work is shown in (c).

and CPE_{ct} correspond to the charge transfer resistance and double-layer capacitance; and W represents the Warburg impedance directly related to lithium-ion diffusion resistance. Due to the instability of carbonate-based electrolyte at high voltage and the reactivity between the charged LNMCO electrode and electrolyte, the formation of a thick SEI layer and deterioration of the surface structure might happen during cycling.[42,46] Figure 9a shows that the SEI resistance of the LNMCO electrode remarkably increases from 95.7 to 689.2 Ω, indicating severe electrolyte decomposition and formation of the thick SEI layer during cycling at high voltage. Moreover, the R_{ct} value of the LNMCO electrode also shows a great increment from 3429 to 22 020 Ω after 50 cycles.

Two reasons may account for such a significant R_{ct} increment. First, the interfacial reaction between the M^{4+} (M = Mn, Co, or Ni) and electrolyte deteriorates surface charge transfer. Second, due to the structure instability of LNMCO, a transition metal ion might migrate from the transition layer to the lithium layer which impedes lithium diffusion at both the surface and bulk LNMCO.[46,47] With the PI coating layer on the surface, the initial SEI resistance of the PI-LNMCO-450

electrode was larger (159.3 Ω) than that of the pristine LNMCO electrode. However, because of the suppression of aggressive side reactions between the electrode and electrolyte by the PI coating layer, the PI-LNMCO-450 electrode exhibited a smaller SEI layer resistance (408 Ω) and charge transfer resistance (8458 Ω) than that of the LNMCO electrode after 50 cycles. The EIS results indicate that the PI layer can separate electrode material from electrolyte and effectively stabilize the electrode/electrolyte interface, leading to better cyclic and rate performances.

4. CONCLUSIONS

A thin PI coating layer (~3 nm) was successfully coated on the surface of LNMCO by a PAA coating after the thermal imidization process. The thermal treatment temperature of PAA-coated LNMCO played a key role on the imidization of the PAA layer which remarkably affected the interaction between the PI layer and LNMCO. Only partial PAA was converted to PI on the surface of PI-LNMCO treated at 300 °C, while the PI-LNMCO treated at 450 °C was featured with a partial reduction of Mn(IV) to Mn(III) caused by charge transfer between the PI layer and LNMCO. The electrochemical performances of PI-LNMO-450 including cyclic stability and rate capability were obviously improved, compared with LNMCO. The PI coating layer effectively separated LNMCO from the electrolyte and stabilized the electrode/electrolyte interface at high voltage ($\geq$4.5 V), leading to a better cyclic performance. Moreover, a partial reduction of Mn(IV) to Mn(III) benefited the migration of polarons, resulting in a higher rate performance.

■ ASSOCIATED CONTENT

ⓢ Supporting Information

The XPS spectra C 1s (a), O 1s (b), and N 1s (c) of the PI-300 and PI-450 membranes. Raman spectra in the range of 1200−1800 cm^{-1} for LNMCO, PI-LNMCO-300, and PI-LNMCO-450. This material is available free of charge via the Internet at http://pubs.acs.org.

■ AUTHOR INFORMATION

Corresponding Author
*E-mail: wangjiulin@sjtu.edu.cn. Tel.: (+86)21-54745887. Fax: (+86)21-54747667.

Notes
The authors declare no competing financial interest.

■ ACKNOWLEDGMENTS

■ REFERENCES

(1) Goodenough, J. B. Electrochemical Energy Storage in a Sustainable Modern Society. *Energy Environ. Sci.* **2014**, 7, 14−18.
(2) Venkateswara Rao, C.; Leela Mohana Reddy, A.; Ishikawa, Y.; Ajayan, P. M. LiNi$_{1/3}$Co$_{1/3}$Mn$_{1/3}$O$_2$-Graphene Composite as a Promising Cathode for Lithium-Ion Batteries. *ACS Appl. Mater. Interfaces* **2011**, 3, 2966−2972.
(3) Li, D.; Kato, Y.; Kobayakawa, K.; Noguchi, H.; Sato, Y. Preparation and Electrochemical Characteristics of Li-Ni$_{1/3}$Mn$_{1/3}$Co$_{1/3}$O$_2$ Coated with Metal Oxides Coating. *J. Power Sources* **2006**, 160, 1342−1348.
(4) Lin, B.; Wen, Z.; Gu, Z.; Huang, S. Morphology and Electrochemical Performance of Li[Ni$_{1/3}$Co$_{1/3}$Mn$_{1/3}$]O$_2$ Cathode

Material by a Slurry Spray Drying Method. *J. Power Sources* 2008, *175*, 564−569.

(5) Guo, D.; Chang, Z.; Tang, H.; Li, B.; Xu, X.; Yuan, X.-Z.; Wang, H. Electrochemical Performance of Solid Sphere Spinel LiMn2O4 with High Tap Density Synthesized by Porous Spherical Mn₃O₄. *Electrochim. Acta* 2014, *123*, 254−259.

(6) Qing, C.; Bai, Y.; Yang, J.; Zhang, W. Enhanced Cycling Stability of LiMn₂O₄ Cathode by Amorphous FePO₄ Coating. *Electrochim. Acta* 2011, *56*, 6612−6618.

(7) Liu, T.; Li, Z.; Wang, D.; Zhu, J.; Wang, B.; Guo, C. The Composite Electrode of LiFePO₄ Cathode Materials Modified with Exfoliated Graphene from Expanded Graphite for High Power Li-ion Batteries. *J. Mater. Chem. A* 2014, *2*, 2822−2829.

(8) Armstrong, A. R.; Holzapfel, M.; Novak, P.; Johnson, C. S.; Kang, S.-H.; Thackeray, M. M.; Bruce, P. G. Demonstrating Oxygen Loss and Associated Structural Reorganization in the Lithium Battery Cathode Li[Ni₀.₂Li₀.₂Mn₀.₆]O₂. *J. Am. Chem. Soc.* 2006, *128*, 8694−8698.

(9) Thackeray, M. M.; Kang, S.-H.; Johnson, C. S.; Vaughey, J. T.; Benedek, R.; Hackney, S. A. Li₂MnO₃-Stabilized LiMO₂ (M = Mn, Ni, Co) Electrodes for Lithium-ion Batteries. *J. Mater. Chem.* 2007, *17*, 3112−3125.

(10) Zheng, J.; Wu, X.; Yang, Y. Improved Electrochemical Performance of Li[Li₀.₂Mn₀.₅₄Ni₀.₁₃Co₀.₁₃]O₂ Cathode Material by Fluorine Incorporation. *Electrochim. Acta* 2013, *105*, 200−208.

(11) Liu, J.; Wang, R.; Xia, Y. Degradation and Structural Evolution of xLi₂MnO₃·(1-x)LiMn₁/₃Ni₁/₃Co₁/₃O₂ during Cycling. *J. Electrochem. Soc.* 2013, *161*, A160−A167.

(12) Zheng, J.; Shi, W.; Gu, M.; Xiao, J.; Zuo, P.; Wang, C.; Zhang, J. G. Electrochemical Kinetics and Performance of Layered Composite Cathode Material Li[Li₀.₂Ni₀.₂Mn₀.₆]O₂. *J. Electrochem. Soc.* 2013, *160*, A2212−A2219.

(13) Yu, X.; Lyu, Y.; Gu, L.; Wu, H.; Bak, S.-M.; Zhou, Y.; Amine, K.; Ehrlich, S. N.; Li, H.; Nam, K.-W.; Yang, X.-Q., Understanding the Rate Capability of High-Energy-Density Li-Rich Layered Li₁.₂Ni₀.₁₅Co₀.₁Mn₀.₅₅O₂ Cathode Materials. *Adv. Energy Mater.* DOI: 10.1002/aenm.201300950.

(14) Yang, X.; Wang, X.; Wei, Q.; Shu, H.; Liu, L.; Yang, S.; Hu, B.; Song, Y.; Zou, G.; Hu, L.; Yi, L. Synthesis and Characterization of a Li-Rich Layered Cathode Material Li₁.₁₅[(Mn₁/₃Ni₁/₃Co₁/₃)₀.₅(Ni₁/₄Mn₃/₄)₀.₅]₀.₈₅O₂ with Spherical Core−Shell Structure. *J. Mater. Chem.* 2012, *22*, 19666−19672.

(15) Yang, X.; Wang, X.; Zou, G.; Hu, L.; Shu, H.; Yang, S.; Liu, L.; Hu, H.; Yuan, H.; Hu, B.; Wei, Q.; Yi, L. Spherical Lithium-Rich Layered Li₁.₁₃[Mn₀.₅₃₄Ni₀.₂₃₃Co₀.₂₃₃]₀.₈₇O₂ with Concentration-Gradient Outer Layer as High-Performance Cathodes for Lithium Ion Batteries. *J. Power Sources* 2013, *232*, 338−347.

(16) Zhang, X.; Belharouak, I.; Li, L.; Lei, Y.; Elam, J. W.; Nie, A.; Chen, X.; Yassar, R. S.; Axelbaum, R. L. Structural and Electrochemical Study of Al₂O₃ and TiO₂ Coated Li₁.₂Ni₀.₁₃Mn₀.₅₄Co₀.₁₃O₂ Cathode Material Using ALD. *Adv. Energy Mater.* 2013, *3*, 1299−1307.

(17) Zhao, J.; Aziz, S.; Wang, Y. Hierarchical Functional Layers on High-Capacity Lithium-Excess Cathodes for Superior Lithium Ion Batteries. *J. Power Sources* 2014, *247*, 95−104.

(18) Wu, F.; Wang, Z.; Su, Y.; Yan, N.; Bao, L.; Chen, S. Li[Li₀.₂Mn₀.₅₄Ni₀.₁₃Co₀.₁₃]O₂-MoO₃ Composite Cathodes with Low Irreversible Capacity Loss for Lithium Ion Batteries. *J. Power Sources* 2014, *247*, 20−25.

(19) Sun, Y.-K.; Lee, M.-J.; Yoon, C. S.; Hassoun, J.; Amine, K.; Scrosati, B. The Role of AlF₃ Coatings in Improving Electrochemical Cycling of Li-Enriched Nickel-Manganese Oxide Electrodes for Li-Ion Batteries. *Adv. Mater.* 2012, *24*, 1192−1196.

(20) Park, J.-H.; Cho, J.-H.; Kim, J.-S.; Shim, E.-G.; Lee, S.-Y. High-Voltage Cell Performance and Thermal Stability of Nanoarchitectured Polyimide Gel Polymer Electrolyte-Coated LiCoO₂ Cathode Materials. *Electrochim. Acta* 2012, *86*, 346−351.

(21) Park, J.-H.; Kim, J.-S.; Shim, E.-G.; Park, K.-W.; Hong, Y. T.; Lee, Y.-S.; Lee, S.-Y. Polyimide Gel Polymer Electrolyte-Nano-

encapsulated LiCoO₂ Cathode Materials for High-Voltage Li-Ion Batteries. *Electrochem. Commun.* 2010, *12*, 1099−1102.

(22) Park, J.-H.; Cho, J.-H.; Kim, S.-B.; Kim, W.-S.; Lee, S.-Y.; Lee, S.-Y. A Novel Ion-Conductive Protection Skin Based on Polyimide Gel Polymer Electrolyte: Application to Nanoscale Coating Layer of High Voltage LiNi₁/₃Co₁/₃Mn₁/₃O₂ Cathode Materials for Lithium-Ion Batteries. *J. Mater. Chem.* 2012, *22*, 12574−12581.

(23) Park, J.-H.; Cho, J.-H.; Lee, E.-H.; Kim, J.-M.; Lee, S.-Y. Thickness-Tunable Polyimide Nanoencapsulating Layers and their Influence on Cell Performance/Thermal Stability of High-Voltage LiCoO₂ Cathode Materials for Lithium-Ion Batteries. *J. Power Sources* 2013, *244*, 442−449.

(24) Zhang, J.; Wang, J.; Yang, J.; NuLi, Y. Artificial Interface Deriving from Sacrificial Tris(trimethylsilyl)phosphate Additive for Lithium Rich Cathode Materials. *Electrochim. Acta* 2014, *117*, 99−104.

(25) Lu, Q.; Fang, J.; Yang, J.; Feng, X.; Wang, J.; Nuli, Y. A Polyimide Ion-Conductive Protection Layer to Suppress Side Reactions on Li₄Ti₅O₁₂ Electrodes at Elevated Temperature. *RSC Adv.* 2014, *4*, 10280−10283.

(26) Mohanty, D.; Sefat, A. S.; Kalnaus, S.; Li, J.; Meisner, R. A.; Payzant, E. A.; Abraham, D. P.; Wood, D. L.; Daniel, C. Investigating Phase Transformation in the Li₁.₂Co₀.₁Mn₀.₅₅Ni₀.₁₅O₂ Lithium-Ion Battery Cathode during High-Voltage Hold (4.5 V) via Magnetic, X-ray Diffraction and Electron Microscopy Studies. *J. Mater. Chem. A* 2013, *1*, 6249−6261.

(27) Wang, C.-C.; Jarvis, K. A.; Ferreira, P. J.; Manthiram, A. Effect of Synthesis Conditions on the First Charge and Reversible Capacities of Lithium-Rich Layered Oxide Cathodes. *Chem. Mater.* 2013, *25*, 3267−3275.

(28) Zhang, L.; Borong, W.; Ning, L.; Feng, W. Hierarchically Porous Micro-Rod Lithium-Rich Cathode Material Li₁.₂Ni₀.₁₃Mn₀.₅₄Co₀.₁₃O₂ for High Performance Lithium-Ion Batteries. *Electrochim. Acta* 2014, *118*, 67−74.

(29) Han, E.; Wu, D.; Qi, S.; Tian, G.; Niu, H.; Shang, G.; Yan, X.; Yang, X. Incorporation of Silver Nanoparticles into the Bulk of the Electrospun Ultrafine Polyimide Nanofibers via a Direct Ion Exchange Self-Metallization Process. *ACS Appl. Mater. Interfaces* 2012, *4*, 2583−2590.

(30) Wu, H.; Wang, K.; Meng, Y.; Lu, K.; Wei, Z. An Organic Cathode Material Based on a Polyimide/CNT Nanocomposite for Lithium Ion Batteries. *J. Mater. Chem. A* 2013, *1*, 6366−6372.

(31) Fu, Q.; Du, F.; Bian, X.; wang, y.; Yan, X.; zhang, y.; zhu, k.; Chen, G.; Wang, C.; wei, y. Electrochemical Performance and Thermal Stability of Li₁.₁₈Co₀.₁₅Ni₀.₁₅Mn₀.₅₂O₂ by Surface Coating with the Li₃VO₄ Ionic Conductor. *J. Mater. Chem. A* 2014, *2*, 7555−7562.

(32) Li, D.; Lian, F.; Hou, X.-m.; Chou, K.-c. Reaction Mechanisms for 0.5Li₂MnO₃·0.5LiMn₀.₅Ni₀.₅O₂ Precursor Prepared by Low-Heating Solid State Reaction. *Int. J. Miner., Metall. Mater.* 2012, *19*, 856−862.

(33) Xiao, F.; Wang, K.; Zhan, M. Atomic Oxygen Erosion Resistance of Titania-Polyimide Hybrid Films Derived from Titanium Tetrabutoxide and Polyamic Acid. *J. Appl. Polym. Sci.* 2012, *123*, 143−151.

(34) Chen, Y.; Xu, G.; Li, J.; Zhang, Y.; Chen, Z.; Kang, F. High Capacity 0.5Li₂MnO₃·0.5LiNi₀.₃₃Co₀.₃₃Mn₀.₃₃O₂ Cathode Material via a Fast Co-Precipitation Method. *Electrochim. Acta* 2013, *87*, 686−692.

(35) Qiao, Q. Q.; Zhang, H. Z.; Li, G. R.; Ye, S. H.; Wang, C. W.; Gao, X. P. Surface Modification of Li-Rich Layered Li-(Li₀.₁₇Ni₀.₂₅Mn₀.₅₈)O₂ Oxide with Li-Mn-PO₄ as the Cathode for Lithium-Ion Batteries. *J. Mater. Chem. A* 2013, *1*, 5262−5268.

(36) Ke, F.; Song, N.; Liang, D.; Xu, H. A Method to Break Charge Transfer Complex of Polyimide: A Study on Solution Behavior. *J. Appl. Polym. Sci.* 2013, *127*, 797−803.

(37) Fu, C.; Li, G.; Luo, D.; Zheng, J.; Li, L. Gel-Combustion Synthesis of Li₁.₂Mn₀.₄Co₀.₄O₂ Composites with High Capacity and Superior Rate Capability for Lithium-Ion Batteries. *J. Mater. Chem. A* 2014, *2*, 1471−1483.

(38) Amalraj, F.; Talianker, M.; Markovsky, B.; Burlaka, L.; Leifer, N.; Goobes, G.; Erickson, E. M.; Haik, O.; Grinblat, J.; Zinigrad, E.;

Aurbach, D.; Lampert, J. K.; Shin, J. Y.; Schulz-Dobrick, M.; Garsuch, A. Studies of Li and Mn-Rich $Li_x[MnNiCo]O_2$ Electrodes: Electrochemical Performance, Structure, and the Effect of the Aluminum Fluoride Coating. *J. Electrochem. Soc.* **2013**, *160*, A2220−A2233.

(39) Wu, Y.; Ming, J.; Zhuo, L.; Yu, Y.; Zhao, F. Simultaneous Surface Coating and Chemical Activation of the Li-Rich Solid Solution Lithium Rechargeable Cathode and its Improved Performance. *Electrochim. Acta* **2013**, *113*, 54−62.

(40) Yu, S.-H.; Yoon, T.; Mun, J.; Park, S.; Kang, Y.-S.; Park, J.-H.; Oh, S. M.; Sung, Y.-E. Continuous Activation of Li_2MnO_3 Component upon Cycling in $Li_{1.167}Ni_{0.233}Co_{0.100}Mn_{0.467}Mo_{0.033}O_2$ Cathode Material for Lithium Ion Batteries. *J. Mater. Chem. A* **2013**, *1*, 2833−2839.

(41) Xiang, X.; Li, X.; Li, W. Preparation and Characterization of Size-Uniform $Li[Li_{0.131}Ni_{0.304}Mn_{0.565}]O_2$ Particles as Cathode Materials for High Energy Lithium Ion Battery. *J. Power Sources* **2013**, *230*, 89−95.

(42) Martha, S. K.; Nanda, J.; Veith, G. M.; Dudney, N. J. Surface Studies of High Voltage Lithium Rich Composition:- $Li_{1.2}Mn_{0.525}Ni_{0.175}Co_{0.1}O_2$. *J. Power Sources* **2012**, *216*, 179−186.

(43) Bordeneuve, H.; Guillemet-Fritsch, S.; Rousset, A.; Schuurman, S.; Poulain, V. Structure and Electrical Properties of Single-Phase Cobalt Manganese Oxide Spinels $Mn_{3-x}Co_xO_4$ Sintered Classically and by Spark Plasma Sintering (SPS). *J. Solid State Chem.* **2009**, *182*, 396−401.

(44) Abouimrane, A.; Compton, O. C.; Deng, H.; Belharouak, I.; Dikin, D. A.; Nguyen, S. T.; Amine, K. Improved Rate Capability in a High-Capacity Layered Cathode Material via Thermal Reduction. *Electrochem. Solid-State Lett.* **2011**, *14*, A126−A129.

(45) Cho, J.-H.; Park, J.-H.; Lee, M.-H.; Song, H.-K.; Lee, S.-Y. A Polymer Electrolyte-Skinned Active Material Strategy toward High-Voltage Lithium Ion Batteries: a Polyimide-Coated $LiNi_{0.5}Mn_{1.5}O_4$ Spinel Cathode Material Case. *Energy Environ. Sci.* **2012**, *5*, 7124−7131.

(46) Abouimrane, A.; Odom, S. A.; Tavassol, H.; Schulmerich, M. V.; Wu, H.; Bhargava, R.; Gewirth, A. A.; Moore, J. S.; Amine, K. 3-Hexylthiophene as a Stabilizing Additive for High Voltage Cathodes in Lithium-Ion Batteries. *J. Electrochem. Soc.* **2012**, *160*, A268−A271.

(47) Xu, B.; Fell, C. R.; Chi, M.; Meng, Y. S. Identifying Surface Structural Changes in Layered Li-Excess Nickel Manganese Oxides in High Voltage Lithium Ion Batteries: A Joint Experimental and Theoretical Study. *Energy Environ. Sci.* **2011**, *4*, 2223−2233.